Unsteady Flamelet Modeling of Soot Formation in Turbulent Diffusion Flames

H. Pitsch
Department of Applied Mechanics and Engineering Science
Center for Energy and Combustion Research, University of California San Diego
La Jolla, CA 92093-0411
e-mail: hpitsch@ames.ucsd.edu

E. Riesmeier, N. Peters
Institut für Technische Mechanik, RWTH Aachen, Templergraben 64, D-52062 Aachen
e-mail: E.Riesmeier@itm.rwth-aachen.de, N.Peters@itm.rwth-aachen.de

Keywords: turbulent diffusion flame, soot formation, flamelet model

Corresponding author:
Heinz Pitsch
Center for Integrated Turbulence Simulations
Flow Physics and Computation Division
Department of Mechanical Engineering
Stanford University
Stanford, CA 94305-3030
Tel: (650) 725-6635
FAX: (650) 725-7834
E-mail: H.Pitsch@stanford.edu

Presented at the 17$^{\text{th}}$ International Colloquium on the Dynamics of Explosions and Reactive Systems

Combustion, Science, and Technology, 158, pp. 389-406, 2000

Unsteady Flamelet Modeling of Soot Formation in Turbulent Diffusion Flames

H. Pitsch, E. Riesmeier, N. Peters

Abstract

The unsteady flamelet model is applied in a numerical simulation of soot formation in a turbulent C_2H_4 jet diffusion flame. A kinetically based soot model is used, which relies on a detailed kinetic mechanism to describe the formation of small polycyclic aromatic hydrocarbons. To describe the formation, growth, and oxidation of soot particles, flamelet equations for the statistical moments of the particle size distribution are derived. Since the effective Lewis number of large particles tends to infinity, a formulation is given, which allows the investigation of the effect of different diffusion coefficients of the particles on the soot formation process. The results of the calculation are compared to experimental data, showing very good agreement for the temperature, which is shown to depend strongly on soot and gas radiation. The predicted soot volume fraction compares reasonably well with the measured data, if differential diffusion of the particles is considered. Calculations with unity particle Lewis numbers show similar results, but overpredicts the soot volume fraction in the rich part of the flame.

Introduction

The formation of soot is one of the most complex problems in combustion science, still by far not well understood. However, intense experimental and theoretical research within the last two decades has improved the fundamental understanding and led to a detailed picture of the soot formation process. This effort has been reviewed for instance by Haynes and Wagner (1981), Bockhorn (1994) and Kennedy (1997).

Soot is commonly believed to be formed by coagulation of polycyclic aromatic hydrocarbon (PAH) species. The resulting small particles essentially grow by heterogeneous surface reactions with acetylene being the most important growth species. These reactions are commonly modeled by the so called H-Abstraction-Carbon-Addition (HACA) mechanism (Frenklach and Wang 1990). The oxidation of soot particles occurs mainly by heterogeneous reactions with OH radicals and molecular oxygen.

In practical devices of technical relevance, such as Diesel engines and gas turbines, soot formation occurs essentially under turbulent conditions. Hence, predictions of soot in numerical simulations become even more difficult because of unresolved questions in the treatment of turbulence/chemistry interactions. Even though some progress has been made recently, applying for instance pdf (Saxena and Pope 1998) or flamelet methods (Pitsch, Chen and Peters 1998, Pitsch 1999) in turbulent jet diffusion flames, many problems remain, including for example the relative importance of molecular transport and differential diffusion.

Differential diffusion has been discussed in the frame of the unsteady flamelet model in a recent paper (Pitsch 1999) showing strong influence on mass fraction development of some species in a methane/hydrogen flame, because of the enhanced diffusivity of hydrogen compared to methane in a laminar region close to the nozzle. For soot particles a similar effect can be expected, even though the laminar near field region does not influence the soot particles, because the formation of soot occurs farther downstream. However, even if the transport in the diffusion flame is essentially governed by turbulence, the particle formation and growth occurs in the reaction zone, which is believed to be thin compared to the turbulent scales, thereby revealing a laminar structure. Since the Lewis numbers of soot particles tend to infinity, the effective diffusivities become negligibly small.

In the present study numerical simulations of soot formation in a turbulent non-premixed jet flame are presented. The unsteady flamelet model is

used to describe chemistry/turbulence interactions. The formation and oxidation of soot is described by a detailed, kinetically based soot model, which is incorporated in the flamelet model. Different assumptions for differential diffusion of the soot particles are applied and the results are discussed in a comparison with experimental data provided by Kent and Honnery (1987).

Governing Equations

Based on the idea of separating the numerical solution of the flow field from the solution of the chemistry, the flamelet approach can be applied to model turbulent diffusion flames. Assuming the smallest turbulent scales to be large compared to the reaction zone thickness, the flame sheet reveals the structure of a laminar flame. Introducing the mixture fraction as a conserved scalar Z defined by the solution of the transport equation

$$\rho\frac{\partial Z}{\partial t} + \rho\boldsymbol{v}\cdot\nabla Z - \nabla\cdot(\rho D_Z\nabla Z) = 0 \tag{1}$$

and the boundary conditions of being unity in the fuel stream and zero in the oxidizer stream, the local mixture can be described by a conservation equation revealing no chemical source term (Pitsch and Peters 1998). In Eq. (1) t is the time and $\boldsymbol{v}$ is the velocity vector. The mixture fraction diffusivity D_Z is arbitrary and is defined here from the assumption of a unity mixture fraction Lewis number as

$$D_Z = \frac{\lambda}{\rho c_p}\,, \tag{2}$$

where λ is the heat conductivity, ρ is the density, and c_p the specific heat capacity at constant pressure. The Lewis number of the mixture fraction is defined in accordance to the Lewis number of the chemical species given by

$$\mathrm{Le}_i = \frac{\lambda}{\rho D_i c_p}. \tag{3}$$

In the case of equal Lewis numbers for all chemical species, the mixture fraction definition given by Eqs. (1) and (2) corresponds to an element mixture fraction based definition as for instance given by Masri and Bilger (1988).

The transport equations for the chemical species mass fractions and the temperature can be written in the following form:

$$\rho\frac{\partial Y_i}{\partial t} + \rho\boldsymbol{v}\cdot\nabla Y_i + \nabla\cdot(\rho Y_i\boldsymbol{V_i}) - \dot{m}_i = 0\,,\;\; i = 1,\ldots,N \tag{4}$$

$$\rho\frac{\partial T}{\partial t} + \rho\boldsymbol{v}\cdot\nabla T - \nabla\cdot\left(\frac{\lambda}{c_p}\nabla T\right) + \sum_{k=1}^{N}\frac{c_{p_k}}{c_p}\rho Y_k\boldsymbol{V_k}\cdot\nabla T - \frac{\lambda}{c_p^2}\nabla c_p\cdot\nabla T$$

$$+\frac{1}{c_p}\left(\sum_{k=1}^{N} h_k\dot{m}_k - \dot{q}_R'''\right) = 0 \tag{5}$$

In these equations T is the temperature, N is the number of chemical species, and Y_i, $\boldsymbol{V_i}$, $\dot{m}_i$, c_{p_k}, and h_i are the mass fraction, the diffusion velocity vector, the chemical production rate, the specific heat capacity at constant pressure, and the enthalpy of species i, respectively. The rate of radiative heat loss per unit volume $\dot{q}_R'''$ accounts for gas and soot radiation, and is described by a model for grey, optically thin gases as

$$\dot{q}_R''' = 2\sigma\,(T^4 - T_u^4)\sum_i p_i\,\alpha_{p,i} \tag{6}$$

In this equation σ denotes the Stefan-Boltzmann constant, T_u the ambient temperature and p_i and $\alpha_{p,i}$ are the partial pressure and the Planck mean absorption coefficient of species i, respectively. In this model only contributions of H_2O, CO_2, and soot particles are considered. The sum in Eq. (6) is therefore given as

$$\sum_i p_i\,\alpha_{p,i} = p_{\mathrm{CO_2}}\,\alpha_{p,\mathrm{CO_2}} + p_{\mathrm{H_2O}}\,\alpha_{p,\mathrm{H_2O}} + f_v\,\alpha_{f_v,\mathrm{Soot}}\,, \tag{7}$$

where f_v represents the soot volume fraction described below. The extinction coefficient of soot is taken from Hubbard and Tien (1978).

It is shown in Pitsch and Peters (1998) that using the mixture fraction definition given by Eq. (1), a flamelet formulation for non-unity Lewis numbers can be derived. However, it has been found in many experiments in turbulent jet diffusion flames (Drake, Pitz and Lapp 1986, Bergmann, Meier, Wolff and Stricker 1998) that differential diffusion effects occur only very close to the nozzle. An explanation for this is given in Pitsch (1999). It is argued that in jet diffusion flames the reaction zone close to the nozzle is

located in a laminar region, which makes molecular diffusion the dominant transport mechanism within the mixing layer. Farther downstream these effects are assumed to be small for the flame investigated in the present paper. The following derivation of the model is therefore performed under the assumption of unity Lewis numbers for all chemical species.

Flamelet Equations

Following Peters (1984) and Peters (1987), flamelet equations for the species mass fractions and the temperature can be derived from Eqs. (4) and (5) by applying a universal coordinate transformation and a subsequent asymptotic approximation under the assumption of a thin reaction zone. These equations are given by

$$\rho\frac{\partial Y_i}{\partial t} - \rho\frac{\chi}{2}\frac{\partial^2 Y_i}{\partial Z^2} - \dot{m}_i = 0 \tag{8}$$

$$\rho\frac{\partial T}{\partial t} - \rho\frac{\chi}{2}\frac{\partial^2 T}{\partial Z^2} - \rho\frac{\chi}{2c_p}\left(\sum_{i=1}^{N} c_{p_i}\frac{\partial Y_i}{\partial Z} + \frac{\partial c_p}{\partial Z}\right)\frac{\partial T}{\partial Z} + \frac{1}{c_p}\left(\sum_{i=1}^{N} h_i\dot{m}_i - \dot{q}_R'''\right) = 0\,. \tag{9}$$

Here, the scalar dissipation rate χ, which appears as a diffusion coefficient in mixture fraction space, is defined as

$$\chi = 2D_Z(\nabla Z)^2\,. \tag{10}$$

It has been shown in recent works (Pitsch et al. 1998, Pitsch 1999) that the unsteady term in Eqs. (8) and (9) is important, if slow chemical or physical processes are involved. For the present study the consideration of the unsteadiness is essential because of the strong impact of radiative heat loss on the energy balance and the consideration of soot formation. In order to incorporate these effects in a CFD calculation, an unsteady flamelet model has been proposed (Pitsch et al. 1998). In this model a flamelet is thought to be introduced at the nozzle exit at conditions close to extinction, traveling downstream with the axial velocity conditioned on stoichiometric mixture and undergoing the changes of the scalar dissipation rate. The time t appearing in the flamelet equations can then be interpreted as a Lagrangian time representing the time of flight of the flamelet and can be related to the axial nozzle distance as

$$t = \int_0^x \frac{1}{u(x)\Big|\left(\widetilde{Z} = Z_{\rm st}\right)} dx\,, \tag{11}$$

where $\widetilde{Z}$ is the Favre average of the mixture fraction and $u(x)\Big|\left(\widetilde{Z}=Z_{\mathrm{st}}\right)$ is the axial velocity component at the radial position with stoichiometric mixture fraction.

The scalar dissipation rate, which appears as a new parameter in the flamelet equations, describes the influence of the turbulent flow field on the laminar flame structure, and has to be modeled from the mean quantities.

Analytic expressions for the scalar dissipation rate in different configurations have been derived under simplifying assumptions (Peters 1984, Kim and Williams 1993, Pitsch et al. 1998) and can commonly be expressed as

$$\chi(Z)=\chi_{\mathrm{st}}f(Z)\,, \tag{12}$$

where χ_{st} denotes the scalar dissipation rate at the stoichiometric mixture fraction Z_{st}. Then with a model for the unconditional mean of the scalar dissipation rate (Jones and Whitelaw 1982),

$$\widetilde{\chi}=c_\chi\frac{\widetilde{\varepsilon}}{\widetilde{k}}\widetilde{Z''^2}\quad\text{with}\quad c_\chi=2.0\,, \tag{13}$$

the conditional mean scalar dissipation rate at stoichiometric mixture in each computational cell can be expressed as

$$\langle\chi_{\mathrm{st}}\rangle=\frac{\widetilde{\chi}}{\int\limits_0^1 f(Z)\widetilde{P}(Z)dZ}\,. \tag{14}$$

In the calculation of a jet diffusion flame these values are evaluated in each computational cell, which are averaged over radial slices according to Pitsch et al. (1998) to provide with Eq. (11) unique values as function of the flamelet time. Here, however, as a simpler approach, the conditional mean scalar dissipation rate as function of the mixture fraction has been assumed to be equal to the unconditional value at the mean mixture fraction. This approach has the advantage that the functional dependence $f(Z)$ is not prescibed.

Soot Model

The calculations have been performed with a detailed chemical reaction scheme compiled by Mauss (1998). The mechanism describes the oxidation of the fuel, the formation of higher aliphatic hydrocarbon species and benzene, and the growth of aromatic compounds up to pyrene.

The further planar growth of polycyclic aromatic hydrocarbons (PAH) is assumed to follow a fast H-abstraction-carbon-addition (HACA) reaction sequence (Frenklach and Wang 1990), which has been extended by Mauss, Trilken, Breitbach and Peters (1994). The coagulation of PAH molecules forming three-dimensional structures is regarded as particle inception. The further growth, the oxidation and the motion of those particles is described by the solution of differential equations. In order to derive these transport equations the particle number density can be defined as

$$N_j = \frac{\rho Y_i}{W_j}\,, \tag{15}$$

where the size class j of the particles represents the number of mass units per particle, such that the particle mass can be expressed as

$$m_j = j\, m_1\,. \tag{16}$$

Here, m_1 denotes the smallest mass unit appearing in the soot particle, which corresponds to the mass of C_2, if the mass of hydrogen appearing in the particles is neglected.

Using Eqs. (4) and (15) the transport equations for the soot particle number density can be written as

$$\rho\frac{\partial N_j/\rho}{\partial t} + \rho\boldsymbol{v}\cdot\nabla(N_j/\rho) - \nabla\cdot(\rho D_{p,j}\nabla(N_j/\rho)) - \nabla\cdot\left(0.55\frac{\mu}{T}\frac{N_j}{\rho}\nabla T\right) - \dot{N}_j = 0\,. \tag{17}$$

In this equation the chemical source term $\dot{N}_j$ includes contributions by particle inception, particle coagulation, condensation of PAH on the particle surface, and heterogeneous reactions of the particles with the gas phase leading to soot mass growth and oxidation.

The diffusion coefficient of the particles $D_{p,j}$ appearing in Eq. (17) varies in the free molecular regime with d_j^{-2} (Friedlander 1986), where d_j is the particle diameter of size class j. Thus, if spherical particles are considered, we can write $D_{p,j} = j^{-2/3} D_{p,1}$, and in terms of the Lewis number $\mathrm{Le}_j = j^{2/3}\mathrm{Le}_1$, where Le_1 is the Lewis number of a hypothetical particle of size class $j = 1$. To preserve generality we write

$$\mathrm{Le}_j = j^{\delta}\,, \tag{18}$$

where Le_1 has been assumed to be unity. This implies $\delta = 2/3$ if differential diffusion effects are to be considered in Eq. (18). The assumption of unity

Lewis numbers for all particles leads to $\delta = 0$. Hence, by the use of this notation it can easily be switched between considering and neglecting the effect of different Lewis numbers of the soot particles by changing $\delta = 2/3$ to $\delta = 0$.

In order to solve Eq. (17), following Frenklach and Harris (1998) the method of statistical moments is applied in the following. The statistical moments of the soot particle size distribution are defined as

$$M_r = \sum_{j=1}^{\infty} j^r N_j \qquad r = 0, \ldots, \infty \,. \tag{19}$$

From Eq. (19) and the definition of the size class in Eq. (16) it can easily be seen that the first moment M_0 corresponds to the mean particle number density, and that the second moment M_1 is the total soot mass in units of C_2 per unit volume. With the molecular weight of C_2 $W_{C_2} = 24\,\mathrm{kg/kmole}$ and the density of the soot particles as for instance given by Frenklach and Wang (1994) $\rho_s = 1800\,\mathrm{kg/m^3}$, the soot volume fraction can be related to M_1 as

$$f_v = \frac{W_{C_2}}{\rho_s} M_1 \,. \tag{20}$$

In order to achieve high accuracy an arbitrary number of soot moments can be used for the description of the soot particles. However, in this study only the first two moments are considered. Fractional moments appearing in the subsequent derivation are determined by Lagrangian interpolation.

Introducing the size dependent Lewis number for the particles given in Eq. (18) and the definition of the statistical moments using Eq. (19) into Eq. (17), the transport equations for the statistical moments are given by

$$\rho \frac{\partial M_r/\rho}{\partial t} + \rho \boldsymbol{v} \cdot \nabla (M_r/\rho) - \nabla \cdot (\rho D_{p,1} \nabla (M_{r-\delta}/\rho)) - \nabla \cdot \left(0.55 \frac{\mu}{T} \frac{M_r}{\rho} \nabla T \right) - \dot{M}_r = 0 \,. \tag{21}$$

The transport equations for the statistical moments can also be transformed into a one-dimensional form with Z as independent coordinate. The flamelet equations for the statistical moments of the soot particle size distribution can be obtained as (Pitsch, Wan and Peters 1995)

$$\begin{aligned} &\rho \frac{\partial M_r/\rho}{\partial t} - \rho \frac{\chi}{2} \frac{\partial^2 M_{r-\delta}/\rho}{\partial Z^2} - \frac{0.55}{2} \Pr \frac{\partial}{\partial Z} \left(\frac{M_r \chi}{T} \frac{\partial T}{\partial Z} \right) \\ &- \frac{1}{4} \frac{\partial \rho \chi}{\partial Z} \left[\frac{\partial M_{r-\delta}/\rho}{\partial Z} - \frac{\partial M_r/\rho}{\partial Z} + 0.55 \Pr \frac{M_r/\rho}{T} \frac{\partial T}{\partial Z} \right] - \dot{M}_r = 0 \,. \end{aligned} \tag{22}$$

As mentioned earlier the differential diffusion parameter δ can be used to switch from considering to neglecting differential diffusion by changing the value of δ from $\delta = 2/3$ to $\delta = 0$. If differential diffusion is considered then all terms involving $M_{r-\delta}$ are small and can be neglected. Then, apart from the thermophoretical transport, only one convective term remains as a transport term. This should be demonstrated in an example. If Eq. (22) is formulated for M_1, the quantity $M_{1/3}$ appears in the diffusion term and an additional transport term. This quantity is determined by logarithmic interpolation between M_0 and M_1 as $M_{1/3} = M_0^{2/3} M_1^{1/3}$, yielding the ratio $M_{1/3}/M_1 = (M_0/M_1)^{2/3}$. Since the average number of mass units per particle M_1/M_0 is at least in the order of 10^4, this implies that $M_{1/3}$ is approximately 500 times smaller than M_1, showing that the terms involving this quantity are small.

In the case of $\delta = 0$ the convection terms cancel and flamelet equations of the species type with additional terms for thermophoresis are recovered for the soot moments. However, numerical tests neglecting these terms show that they have only small influence in the investigated configuration.

Numerical Simulation

Kent and Honnery (1987) experimentally investigated a turbulent jet diffusion flame configuration providing the data to verify the numerical models used in this study. Pure ethylene enters the domain through a nozzle with a diameter of $D = 3\,\mathrm{mm}$ issuing into quiescent air with an average exit velocity of $52\,\mathrm{m/s}$. This leads to a jet exit Reynolds number of $\mathrm{Re} = 14660$. The radial velocity distribution is prescribed using the 1/7 power law.

The flow field solution is obtained by using the FLUENT code. This CFD code has been extended by transport equations for the mean and the variance of the mixture fraction

$$\frac{\partial(\bar{\rho}\widetilde{Z})}{\partial t} + \nabla \cdot (\bar{\rho}\boldsymbol{u}\widetilde{Z}) = \nabla \cdot \left[\frac{\mu_t}{\mathrm{Sc}_{\widetilde{Z}}} \nabla \widetilde{Z}\right] \tag{23}$$

$$\frac{\partial(\bar{\rho}\widetilde{Z''^2})}{\partial t} + \nabla \cdot (\bar{\rho}\boldsymbol{u}\widetilde{Z''^2}) = \nabla \cdot \left[\frac{\mu_t}{\mathrm{Sc}_{\widetilde{Z''^2}}} \nabla \widetilde{Z''^2}\right] + \frac{2\mu_t}{\mathrm{Sc}_{\widetilde{Z''^2}}} (\nabla \widetilde{Z})^2 - \bar{\rho}\widetilde{\chi} \tag{24}$$

as well as for the mean enthalpy

$$\frac{\partial(\bar{\rho}\tilde{h})}{\partial t} + \nabla \cdot (\bar{\rho}\boldsymbol{u}\tilde{h}) = \frac{D\tilde{p}}{Dt} - \nabla \cdot \widetilde{\boldsymbol{J}} + \bar{\rho}\tilde{\varepsilon} + \widetilde{\dot{q}'''_R}\,. \tag{25}$$

Here, $\widetilde{\boldsymbol{J}}$ is the turbulent heat flux vector and the enthalpy is defined to include the heat of formation, such that the transport equation has no chemical source term. The turbulent mean value of the scalar dissipation rate appearing in the mixture fraction variance equation is given by Eq. (13).

To determine the turbulent mean values of the species mass fractions $\widetilde{Y}_i$, a presumed pdf for the mixture fraction Z is used. The mixture fraction pdf is assumed to be represented by a β-function, whose shape depends on the spatial distribution of the mean and the variance of the mixture fraction.

Turbulence is modeled by applying a standard $\tilde{k}$-$\tilde{\varepsilon}$ model including buoyancy effects and a round jet correction as proposed by Pope (1978). The calculations have been performed for an axisymmetric domain of 1000 $\times$ 500 mm axial $\times$ radial length on a 200 $\times$ 100 cell non-equidistant mesh.

The unsteady flamelets were computed interactively with the CFD solution. For the flamelet calculations unity Lewis numbers have been assumed for all chemical species.

The initial conditions for the unsteady flamelet have been taken from a steady solution of a burning flamelet using the computed scalar dissipation rate profile, which is closest to the nozzle. However, the exact conditions for the initialization are of minor importance, since it has been shown in Pitsch et al. (1998) that unsteady effects in this region are small.

Results and Discussion

The results of the calculations are compared to the experimental data by Kent and Honnery (1987) in the following. In order to provide an overview of the configuration, two-dimensional fields of the temperature and the soot volume fraction are given. Results will also be shown along the centerline and for radial slices at $x/D = 46$, 80.5, and 115, corresponding to 0.4, 0.7, and 1.0 times the axial distance of the maximum axial laser light extinction in the experiments. Hence, $x/D = 115$ is expected to be the position of maximum soot volume fraction on the centerline. The calculations shown in the following have been performed with the differential diffusion parameter δ defined by Eq. (18) set to $\delta = 2/3$, thereby accounting for different Lewis numbers of the soot particles.

The calculated mean mixture fraction along the centerline is given in Fig. 1. The stoichiometric mixture fraction is $Z_{\mathrm{st}} \approx 0.064$ and reaches the centerline in the current calculations at $x/D = 147$, which is in accordance

with the simulations by Kent and Honnery (1987), where $x_{\mathrm{st}}/D = 153$ has been found.

Figure 2 shows the calculated temperature field, indicating the strong influence of radiation in this particular configuration. The maximum temperature is about $T = 1840\,\mathrm{K}$ and appears around $x/D = 70$ at an off-axis radial position in a very thin layer around stoichiometric mixture. Thereafter the temperature decreases because of radiation, such that the maximum axial temperature is only $T = 1810\,\mathrm{K}$.

This is also shown in Fig. 1, where the computed axial temperature development is compared to the experimental data. The temperature is very well predicted throughout the entire flame. Only in the range between approximately $x/D = 85$–125 the temperature is slightly overpredicted, which will be shown later to result from a slight underprediction of the soot volume fraction. Figure 1 also shows the results from a calculation, where soot radiation has been neglected, while still accounting for gas radiation, and from a calculation neglecting both, soot and gas radiation. The comparison with the actual calculation shows that both contributions influence the maximum temperature by approximately 150–200 K. It is also observed that although soot radiation is proportional to the fourth power of the temperature, it acts mainly on the rich side, where the temperature is actually lower than at stoichiometric mixture, because soot only exists in this part of the flame. The influence on the maximum temperature therefore results from the enhanced diffusive flux of energy to the rich side. Gas radiation on the other hand acts mainly at the maximum temperature, which occurs close to stoichiometric mixture.

The radial temperature profiles at different downstream locations are given in Fig. 3. Again, good agreement with experimental data can be obtained showing that also the off-axis temperature maximum is well predicted. However, the spreading rate of the jet seems to be slightly overestimated for the downstream position.

From these results two first conclusions can be drawn, which give the basis for the further discussion of soot formation: The data provided by Kent and Honnery (1987), which is used in this study to discuss modelling issues of soot formation in turbulent flames includes only data for mean temperature and soot volume fraction, but not for the mixture fraction, which has been shown in the previous sections to be a very important quantity in flamelet models. Therefore, an accurate description of the mixture fraction is essential to draw conclusions about the predictions of soot formation. However, the

very good agreement of the temperature with the experimental data shown in Figs. 1 and 3 will be used as indication that also the mixture fraction is predicted quite accurately. It has also be shown in Fig. 1 that the radiation of soot particles has a very strong influence on the temperature. This strongly supports the quality of the experimentally observed soot volume fraction, since, because of the strong influence of soot radiation, only if the predicted soot volume fraction is in the right order of magnitude also the temperature predictions agree well with the experiments.

The soot volume fraction field obtained from the numerical calculation is given in Fig. 4. The formation of soot starts already very close to the nozzle in a very narrow region around $r/D = 1$. At the centerline soot starts to appear at $x/D = 30$. The soot maximum reaches the centerline at approximately $x/D = 95$, which corresponds to a mixture fraction of $Z = 0.13$. Soot finally disappears at $x/D = 185$, where the mean mixture fraction is approximately $Z = 0.03$.

The predicted soot volume fraction along the centerline is compared to the experimental data in Fig. 5. The maximum value of approximately $f_{v,\max} = 1.7 \cdot 10^{-6}$ is slightly underpredicted. The appearance of soot on the centerline and also the onset of the oxidation process on the centerline are too early leading essentially to an upstream shift of the soot profile. However, the overall shape of the profile seems to be predicted quite accurately. This could be caused by a slightly overpredicted decay rate of the axial mixture fraction profile, which could also explain the disagreement in the temperature profile. However, the available experimental data is not sufficient for a final conclusion.

Figure 6 shows the radial distribution of the soot volume fraction at different downstream locations. Although the centerline value at $x/D = 46$ is in good agreement, the experimentally observed off-axis maximum of soot is largely overpredicted by the model. At $x/D = 80.5$, the comparison looks much better, especially in the lean part of the flame. At $x/D = 115$ the predicted data are already decreasing, thereby underpredicting the soot volume fraction slightly. However, the overall shape of the radial profile is in good agreement with the experiment.

In order to demonstrate the effect of differential diffusion of the soot particles Fig. 5 also shows the soot volume fraction from a calculation using a differential diffusion parameter $\delta = 0$, thereby setting the Lewis numbers of all particle sizes to unity. Because of the strong diffusion of the soot particles out of the very narrow soot formation region the soot is redistributed in

mixture fraction space leading still to a comparable maximum soot volume fraction. However, the diffusion of the particles to the rich part of the flame leads to an even stronger overprediction of the soot volume fraction in this region.

Conclusions

In the present study a detailed soot model has been used in the frame of the unsteady flamelet model for predictions of soot formation in a turbulent jet diffusion flame. The predicted temperature has been shown to be strongly influenced by both, gas and soot radiation, but nevertheless to be in very good agreement with the experimental data. This leads to the conclusions that the mixture fraction field, for which no experimental data is available, also has to be predicted reasonably well, and also that the measured soot volume fraction is likely to be quite accurate because of its strong influence on the temperature. Also the overall agreement of the soot volume fraction with experimental data is quite reasonable. However, soot production close to the nozzle and the oxidation rate downstream of the maximum centerline soot volume fraction are overpredicted. Finally, the influence of differential diffusion on the predicted soot volume fraction is analyzed, showing that numerical predictions for soot accounting for differential diffusion are in better agreement with the experiments, while the unity Lewis number assumption overestimates the measured soot volume fraction in the rich part of the flame. However, it should be mentioned that neither method is proposed as being superior here. The emphasis in this study is to reveal the high sensitivity of the description of transport processes on soot formation. It has been found that the description of soot formation in turbulent flames is much more complicated than predictions of heat release or even the formation of NO_x, which have been investigated in earlier studies, and much more work has to be done in order to achieve a comprehensive understanding of the problem.

References

Bergmann, V., Meier, W., Wolff, D. and Stricker, W.: 1998, Application of spontaneous Raman and Raleigh scattering and 2D LIF for the charac-

terization of a turbulent $CH_4/H_2/N_2$ jet diffusion flame, *Appl. Phys. B* **66**, 489–502.

Bockhorn, H. E.: 1994, *Soot Formation in Combustion*, Springer-Verlag.

Drake, M. C., Pitz, R. W. and Lapp, M.: 1986, Laser measurements on non-premixed H_2-air flames for assessment of turbulent combustion models, *AIAA J.* **24**(6), 905–917.

Frenklach, M. and Harris, S. J.: 1998, Aerosol dynamics modeling using the method of moments, *J. Coll. Interf. Sci.* **66**, 489–502.

Frenklach, M. and Wang, H.: 1990, Detailed modeling of soot particle nucleation and growth, *Twenty-Third Symposium (International) on Combustion*, The Combustion Institute, pp. 1559–1566.

Frenklach, M. and Wang, H.: 1994, Detailed mechanism and modeling of soot particle formation, *in* H. Bockhorn (ed.), *Soot Formation in Combustion*, Springer Verlag, pp. 165–190.

Friedlander, S. K.: 1986, *Smoke, Dust and Haze*, Wiley & Sons.

Haynes, B. S. and Wagner, H. G.: 1981, *Prog. Energy Combust. Sci.* **7**, 229.

Hubbard, G., L. and Tien, C., L.: 1978, Infrared mean absorption coeffiecients of luminous flames and smoke, *J. Heat Transfer* **100**, 235.

Jones, W. P. and Whitelaw, J. H.: 1982, Calculation methods for reacting turbulent flows: A review, *Combust. Flame* **48**, 1.

Kennedy, I.: 1997, *Prog. Energy Combust. Sci.* **23**, 95–132.

Kent, J. H. and Honnery, D.: 1987, Modelling sooting turbulent jet flames using an extended flamelet technique, *Comb. Sci. Tech.* **54**, 383–397.

Kim, J. S. and Williams, F. A.: 1993, Structures of flow and mixture-fraction fields for counterflow diffusion flames with small stoichiometric mixture fractions, *SIAM J. Appl. Math.* **53**, 1551–1566.

Masri, A. R. and Bilger, R. W.: 1988, *Comb. Flame* **73**, 261–285.

Mauss, F.: 1998, *Entwicklung eines kinetischen Modells der Rubildung mit schneller Polymerisation*, PhD thesis, RWTH Aachen.

Mauss, F., Trilken, B., Breitbach, H. and Peters, N.: 1994, Soot formation in partially premixed diffusion flames at atmospheric pressure, *in* H. Bockhorn (ed.), *Soot Formation in Combustion*, Springer Verlag, pp. 325–349.

Peters, N.: 1984, Laminar diffusion flamelet models in non-premixed turbulent combustion, *Prog. Energy Combust. Sci.* **10**, 319–339.

Peters, N.: 1987, Laminar flamelet concepts in turbulent combustion, *Twenty-First Symposium (International) on Combustion*, The Combustion Institute, pp. 1231–1250.

Pitsch, H.: 1999, Unsteady flamelet modeling of differential diffusion in turbulent jet diffusion flames, *Comb. Flame* . submitted.

Pitsch, H., Chen, M. and Peters, N.: 1998, Unsteady flamelet modeling of turbulent hydrogen/air diffusion flames, *Twenty-Seventh Symposium (International) on Combustion*, The Combustion Institute, pp. 1057–1064.

Pitsch, H. and Peters, N.: 1998, A consistent flamelet formulation for non-premixed combustion considering differential diffusion effects, *Comb. Flame* **114**, 26–40.

Pitsch, H., Wan, Y. P. and Peters, N.: 1995, Numerical investigation of soot formation and oxidation under diesel engine conditions, *SAE Paper* **952357**.

Pope, S. B.: 1978, An explanation of the turbulent round-jet/plain-jet anomaly, *AIAA J.* **16**(3), 279–281.

Saxena, V. and Pope, S. B.: 1998, Pdf calculations of major and minor species in a turbulent piloted jet flame, *Twenty-Seventh Symposium (International) on Combustion, The Combustion Institute*, pp. 1081–1086.

List of Figures

Figure 1:

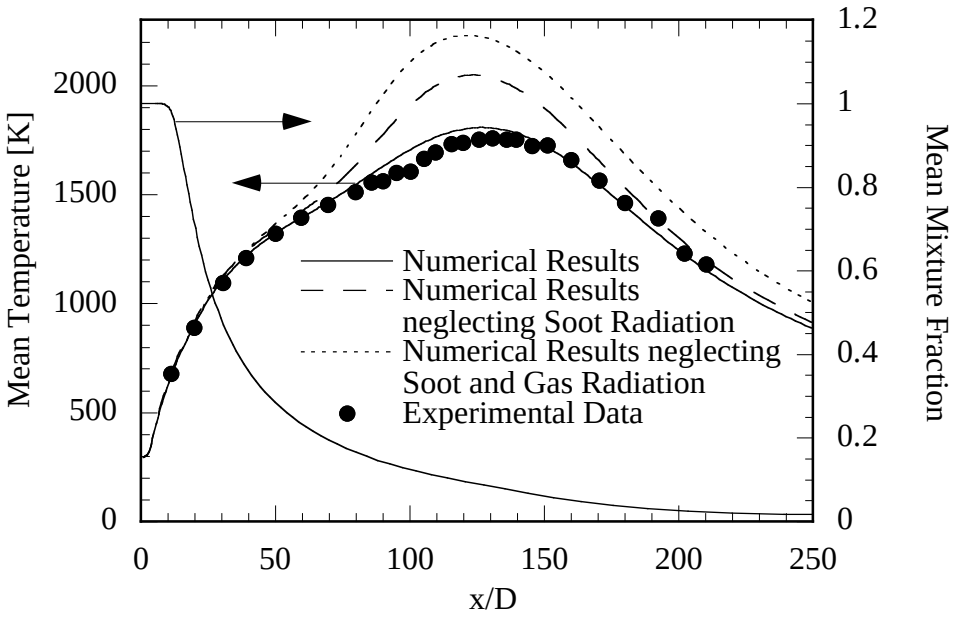
Mean Temperature [K]
Mean Mixture Fraction
x/D
0
500
1000
1500
2000
0
0.2
0.4
0.6
0.8
1
1.2
0
50
100
150
200
250
Numerical Results
Numerical Results neglecting Soot Radiation
Numerical Results neglecting Soot and Gas Radiation
Experimental Data

Figure 2:

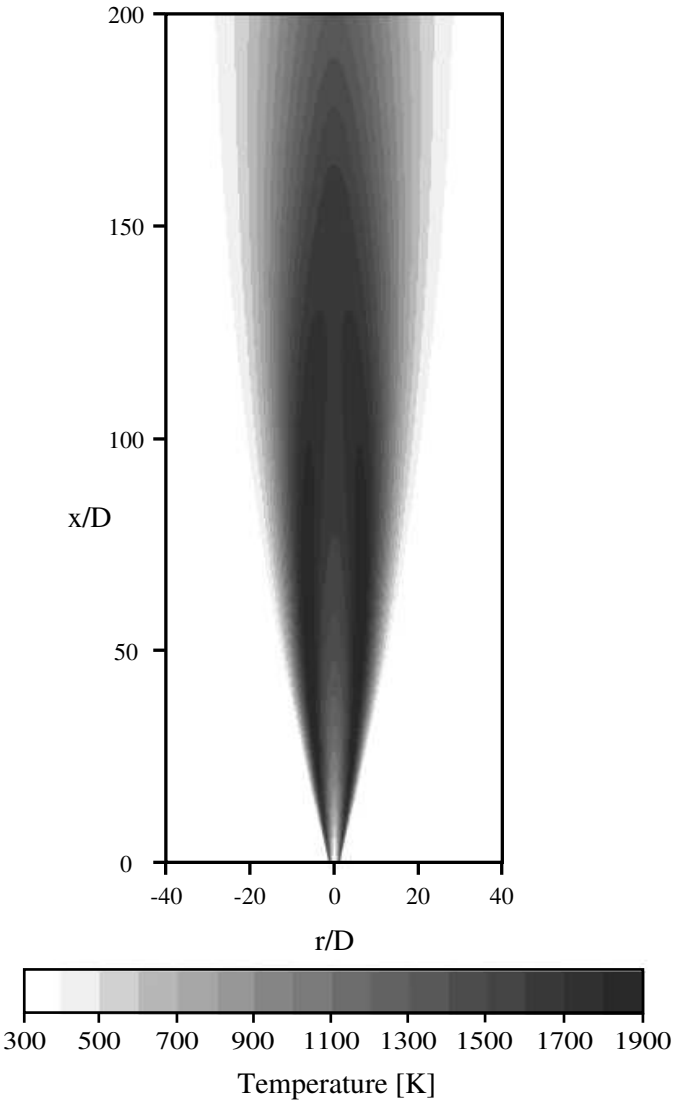
200
150
100
x/D
50
0
-40
-20
0
20
40
r/D
300
500
700
900
1100
1300
1500
1700
1900
Temperature [K]

Figure 3:

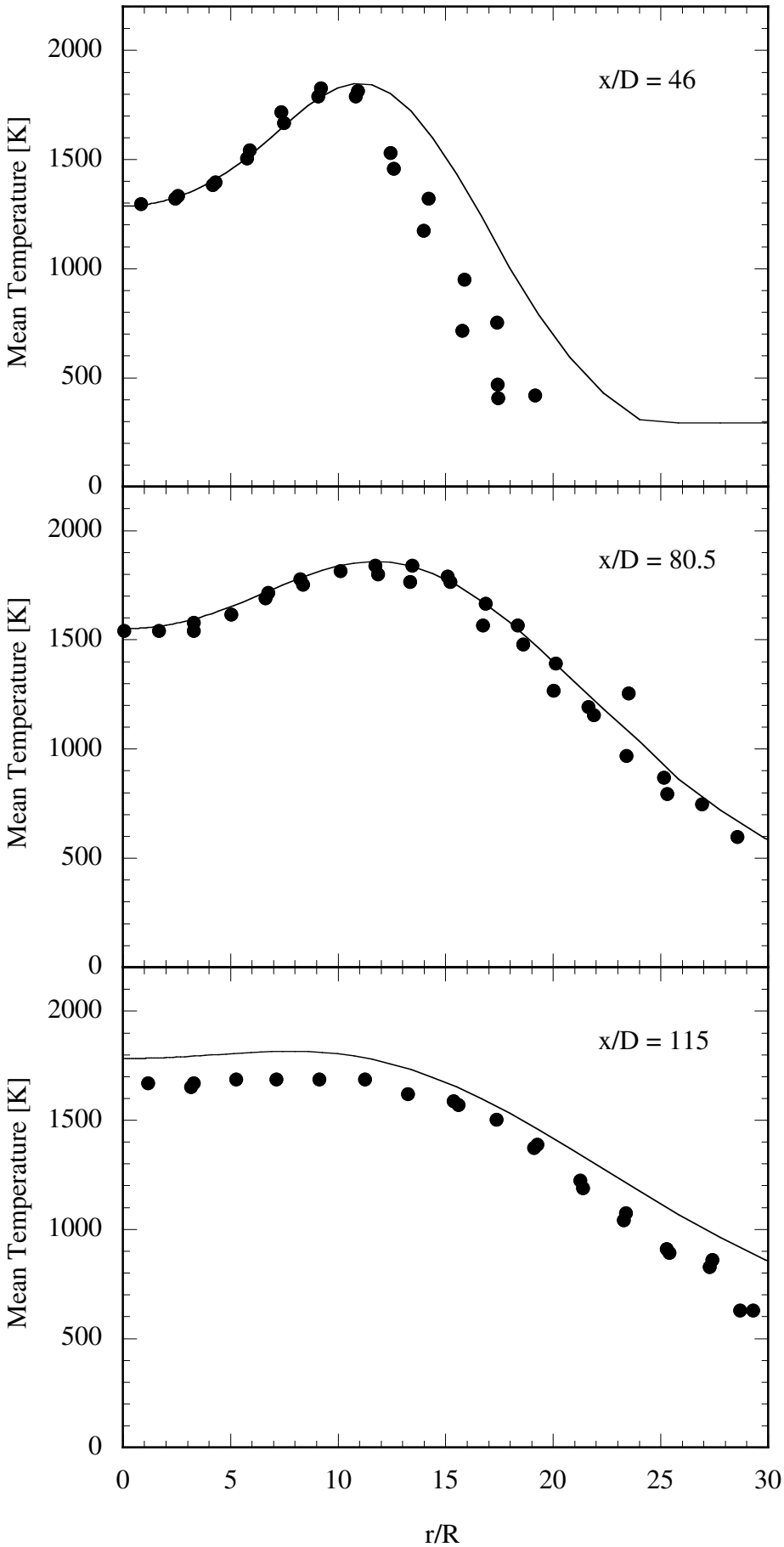
x/D = 46
x/D = 80.5
x/D = 115
Mean Temperature [K]
0
500
1000
1500
2000
0
5
10
15
20
25
30
r/R

Figure 4:

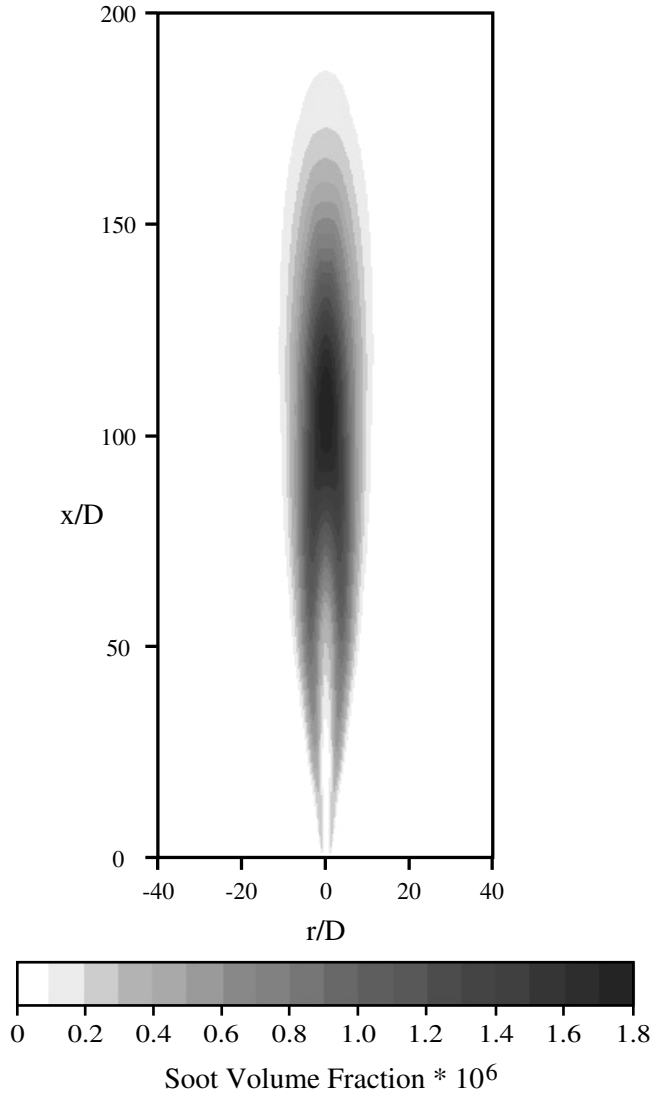
200
150
100
50
0
x/D
-40
-20
0
20
40
r/D
0
0.2
0.4
0.6
0.8
1.0
1.2
1.4
1.6
1.8
Soot Volume Fraction * 10^6

Figure 5:

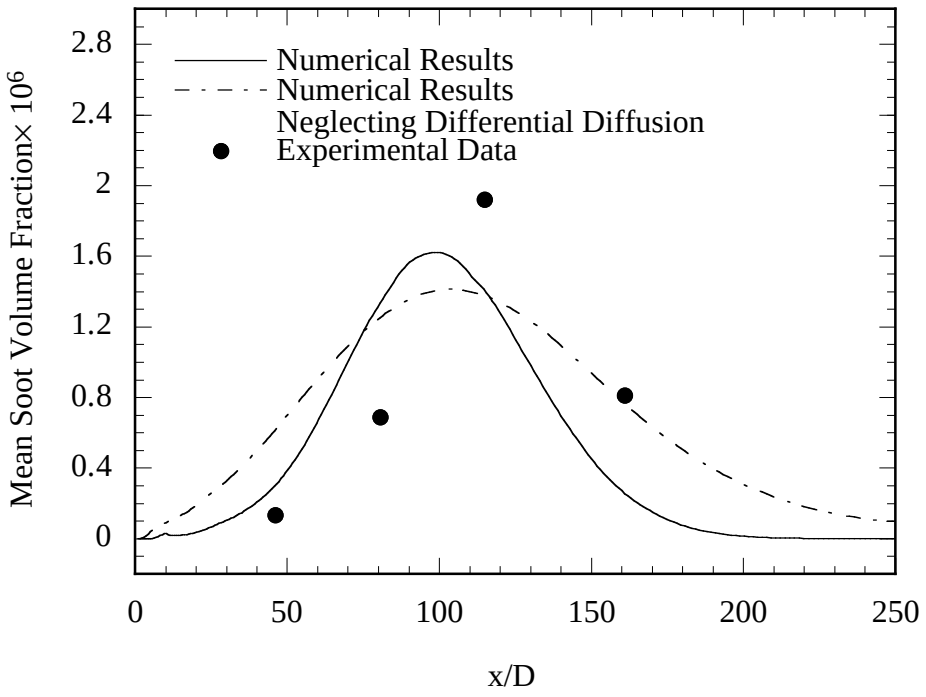
Numerical Results
Numerical Results
Neglecting Differential Diffusion
Experimental Data
Mean Soot Volume Fraction× 10^6
x/D
0
0.4
0.8
1.2
1.6
2
2.4
2.8
0
50
100
150
200
250

Figure 6:

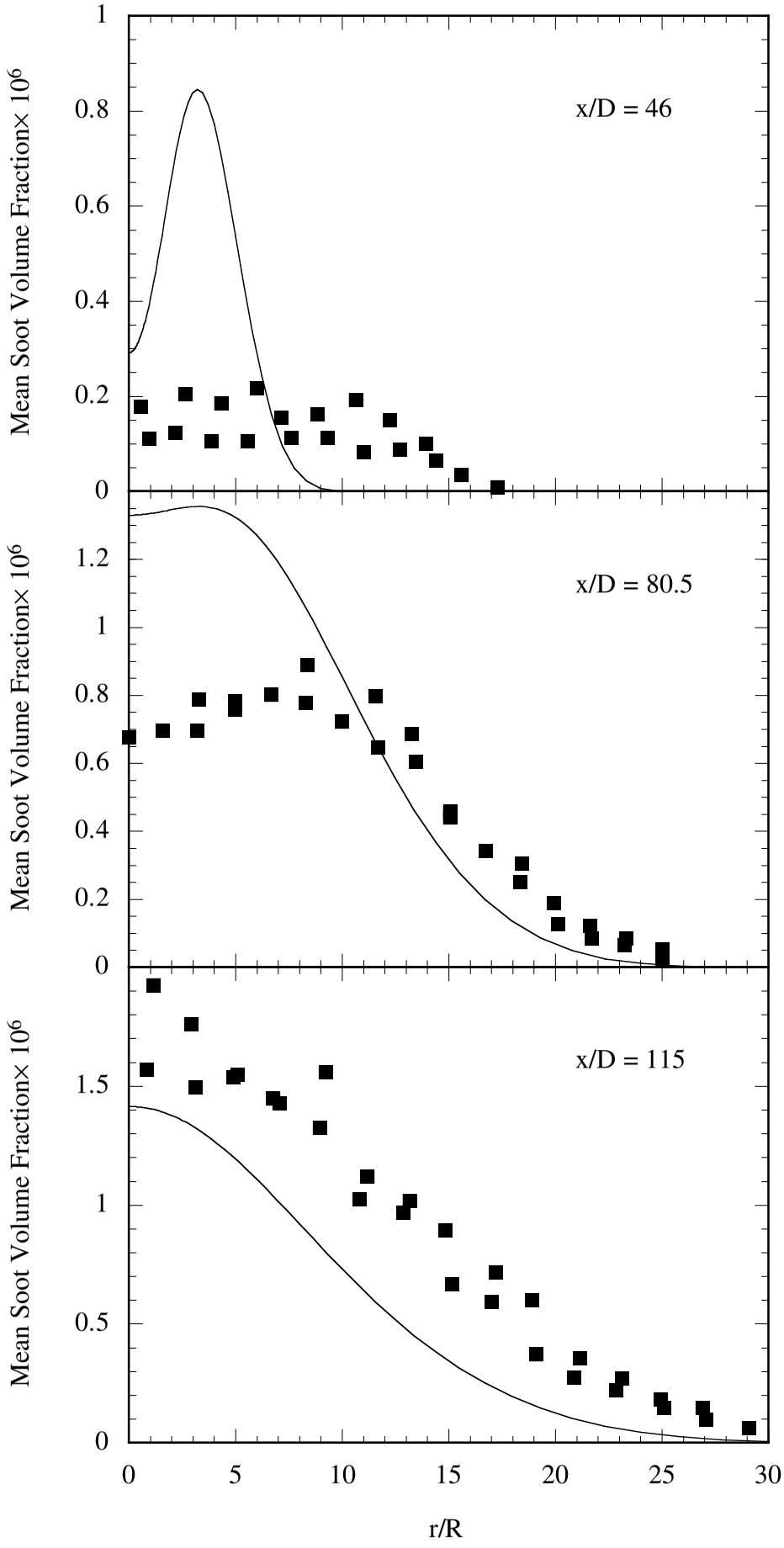
Mean Soot Volume Fraction× 10^6
x/D = 46
x/D = 80.5
x/D = 115
r/R
0
0.2
0.4
0.6
0.8
1
1.2
1.5
5
10
15
20
25
30